Correlated frequency noise in a multimode acoustic resonator

Nuttamas Tubsrinuan [*]

Department of Microtechnology and Nanoscience MC2, Chalmers University of Technology, Göteborg, Sweden
and London Centre for Nanotechnology, University College London, Gordon Street, London WC1H 0AH, United Kingdom

Jared H. Cole

Chemical and Quantum Physics, School of Science, RMIT University, Melbourne, VIC 3001, Australia

Per Delsing

Department of Microtechnology and Nanoscience MC2, Chalmers University of Technology, SE-41296 Göteborg, Sweden

Gustav Andersson [†]

Department of Microtechnology and Nanoscience MC2, Chalmers University of Technology, Göteborg, Sweden
and Pritzker School of Molecular Engineering, University of Chicago, Chicago, Illinois 60637, USA

Frequency instabilities are a major source of errors in quantum devices. This Letter investigates frequency fluctuations in a surface acoustic wave (SAW) resonator, where reflection coefficients of 14 SAW modes are measured simultaneously for more than 7 h. We report two distinct noise characteristics. Multimode frequency noise caused by interactions with two-level system (TLS) defects shows significant degrees of correlation that diminish with increased detuning. This finding agrees with the current understanding of the parasitic TLS behavior as one of the dominant noise sources in quantum devices. In addition to the TLS-induced noise, we observe strong anomalous frequency fluctuations with slow, anticorrelated dynamics. These noise bursts resemble signatures of cosmic radiation observed in superconducting quantum systems.

Decoherence in quantum devices leads to quantum information loss and limits their performance [1,2]. A number of decoherence channels have been identified, including various types of parasitic two-level systems (TLSs) [3,4] and quasiparticles [5]. Quasiparticle generation can be induced by stray infrared light [6] and cosmic radiation [7], while TLS defects inducing loss and noise reside in the circuit [8,9]. Over long timescales, these noise sources impact the stability of device parameters [2,3,10], necessitating frequent calibration or additional mitigation measures [11,12]. In the past decades, significant enhancement in the coherence of superconducting devices has been achieved by improved microwave engineering [13], circuit design [14], fabrication methods [15], and materials [16]. In spite of these developments, decoherence remains a significant issue. A better understanding of noise processes is important in order to mitigate decoherence mechanisms and advance the development of solid state quantum processors.

In this Letter, we use a multifrequency signal (a frequency comb) to simultaneously probe frequency fluctuations in 14 modes of a surface acoustic wave (SAW) resonator at cryogenic temperatures. Tracking the reflection coefficient of the SAW resonator for more than 7 h, we observe that there are two dominant noise processes taking place in the device. We further investigate the noise correlations and their characteristics.

Two-level system defects residing at dielectric surfaces and interfaces of superconducting circuits have been considered a central problem causing frequency fluctuations and significant energy dissipation [4,8,17]. Despite many attempts in the past decades [9], TLS-induced loss and noise remain persistent issues in superconducting quantum processors. Although the microscopic nature of TLSs is not well understood, the standard tunneling model (STM) [9,18,19] has been successfully used as a framework for understanding the TLS interaction with quantum circuits. The STM predicts power-dependent losses and temperature-dependent resonance frequency shifts due to the direct coupling between quantum devices and coherent TLSs, which have transition energies larger than $k_B T$. In addition to coherent TLSs there are thermal fluctuators, two-level systems with sufficiently low transition energies to be thermally activated at millikelvin temperatures. A direct interaction between TLSs is a significant effect not accounted for by the STM [8,20,21]. When coherent TLSs couple with surrounding thermal fluctuators, they are subject to a

---

*nuttamas.tubsrinuan.20@ucl.ac.uk
†gandersson@uchicago.edu

continuous time-dependent energy shift, known as spectral diffusion [22]. While undergoing spectral diffusion, they can couple dispersively to quantum devices, resulting in a frequency drift that translates into phase noise [23,24].

TLSs couple to both electromagnetic [4] and strain fields [25]. Their behaviors have been studied using superconducting qubits [4,21], microwave resonators [26,27], and mechanical resonators [28–30]. A study of a surface acoustic wave (SAW) device at cryogenic temperature reveals that energy losses are caused by the coupling to parasitic TLSs [31]. Further two-tone spectroscopy of TLSs using a SAW resonator shows that TLSs dominate the losses [29], suggesting the potential of SAW resonators for investigating TLSs. Due to the slow propagation, the SAW wavelength is smaller than the electromagnetic wavelength by five orders of magnitude at the same frequency. This characteristic allows SAW resonant structures to accommodate many resonant frequencies in a compact design.

Here, we exploit multiple resonance modes of the SAW resonator to probe frequency noise caused by TLSs at many different frequencies simultaneously. According to the Jaynes-Cummings model [32], the resonance frequency of a resonator f, which is dispersively coupled to an individual TLS, is given by

$$f = f_r + \frac{g^2}{f_r - f_{\text{TLS}}} \hat{\sigma}_z, \tag{1}$$

where $\hat{\sigma}_z$ is the Pauli spin operator acting on the TLS, and g represents the TLS-resonator coupling strength. The resonance frequency of the bare resonator and the TLS are denoted by f_r and f_{TLS}, respectively. In most realistic cases, the resonator interacts with a TLS ensemble with a frequency distribution spanning the resonator bandwidth. The effective frequency shift is the sum of the dispersive shifts contributed by all the individual TLSs. Due to their small wavelengths and high wave numbers, SAW modes are close to each other in frequency and have a large overlap in real space. Thus, all modes interact with the same physical TLS ensemble, however, with slightly different detuning. Therefore, the multimode frequency noise in a SAW resonator is expected to be correlated. Additionally, the degree of correlation should depend on the detuning, as suggested by Eq. (1).

In superconducting devices, cosmic rays and other sources of radiation can generate high-energy phonons [33–35]. These phonons break Cooper pairs, leading to an increased kinetic inductance of the superconducting material and associated resonance frequency shifts [36]. A recent study on superconducting granular aluminum resonators shows that ionizing radiation due to high-energy cosmic rays creates phonons that in turn generate quasiparticle bursts, resulting in resonance frequency shifts and reduced quality factors [37]. This effect has also been observed in transmon qubits with shortened relaxation and dephasing times as a result [7,38,39]. Direct measurements of rare events which were attributed to cosmic rays have also been observed in gravitational wave experiments [40–42]. The frequency noise caused by ionizing radiation can be suppressed by the use of a phonon absorber [43], radiation shielding, and conducting experiments at a deep-underground facility [37].

Our SAW resonator, fabricated on a piezoelectric GaAs substrate, has two Bragg mirrors, located 1440 μm apart. Each mirror has 800 fingers. An interdigital transducer (IDT) is placed at the center of the cavity, serving as both the input and output port. The IDT has a split-finger design with 50 periods of 1.2 μm, as illustrated in Fig. 1(a) [29]. The device supports 14 resonance modes within the frequency range from 2.37 to 2.40 GHz. The free spectral range between each mode is approximately 2 MHz. The characteristics of the SAW resonator are shown in Figs. 1(b) and 1(c). The resonance linewidths are between 18 and 32 kHz. We extract the resonator parameters based on the expression for the reflection coefficient [44],

$$S_{11}(f) = -ae^{-i(\pi-\theta)} \left[1 - \frac{2(Q_L/Q_C)e^{i\phi_0}}{1 + 2iQ_L\left(\frac{f-f_r}{f_r}\right)} \right], \tag{2}$$

where f is the probe frequency and the parameter a is an amplitude scaling coefficient. A phase shift due to cable delay is denoted by θ. The loaded quality factor and the external quality factor are represented by Q_L and Q_C, respectively. An impedance mismatch is accounted for by the parameter ϕ_0. We drive the SAW resonator continuously so that the estimated number of phonons is approximately 1000. The probe frequencies are defined from the resonance frequencies extracted from the resonator profile in Fig. 1(b) using Eq. (2), such that the phase response is maximally sensitive to frequency shifts.

For this device, the quality factors are slightly different for each frequency, as shown in Fig. 1(d). We measure the SAW resonator in the overcoupled regime, where $Q_i > Q_C$. We measure resonance frequency fluctuations by tracking the amplitude and phase response while driving 14 modes of the SAW resonator simultaneously for 2.6×10^4 s, approximately 7 h and 15 min. Additionally, we apply a control tone at 2.41 GHz, off resonant with every SAW mode. This control tone is used as a reference for the signal fluctuations due to other sources in the environment. For details in experimental setup, see Supplemental Material [45]. The long measurement duration is used in order to capture any TLS telegraphic switching. The rates for such events have been observed to be in the range of 75 μHz–2 mHz [2]. We calculate the frequency from the measured reflection coefficient S_{11} using the parameters extracted from the resonance profile in Fig. 1(b) and Eq. (2).

The time traces in Fig. 2(a) show resonance frequency fluctuations of the 14 different modes within the resonator band of 2.37–2.40 GHz. We observe a baseline of frequency fluctuations with uniform amplitude, superimposed with occasional striking large-amplitude fluctuations. There are "quiet" time windows where only small fluctuations are present. For instance, in the time window highlighted in Fig. 2(b), there are no burst events. The noise amplitude is small, 50 Hz on average, compared to the largest fluctuation of 20 kHz. There is no obvious relationship between fluctuations in different modes. For a device having a small mode volume, we would expect to see a clear telegraphic shift caused by an individual TLS [24]. In contrast, our SAW resonator has a large mode volume. Thus, we can observe frequency drifts resulting from many weakly-coupled TLSs, which makes telegraphic features indistinct.
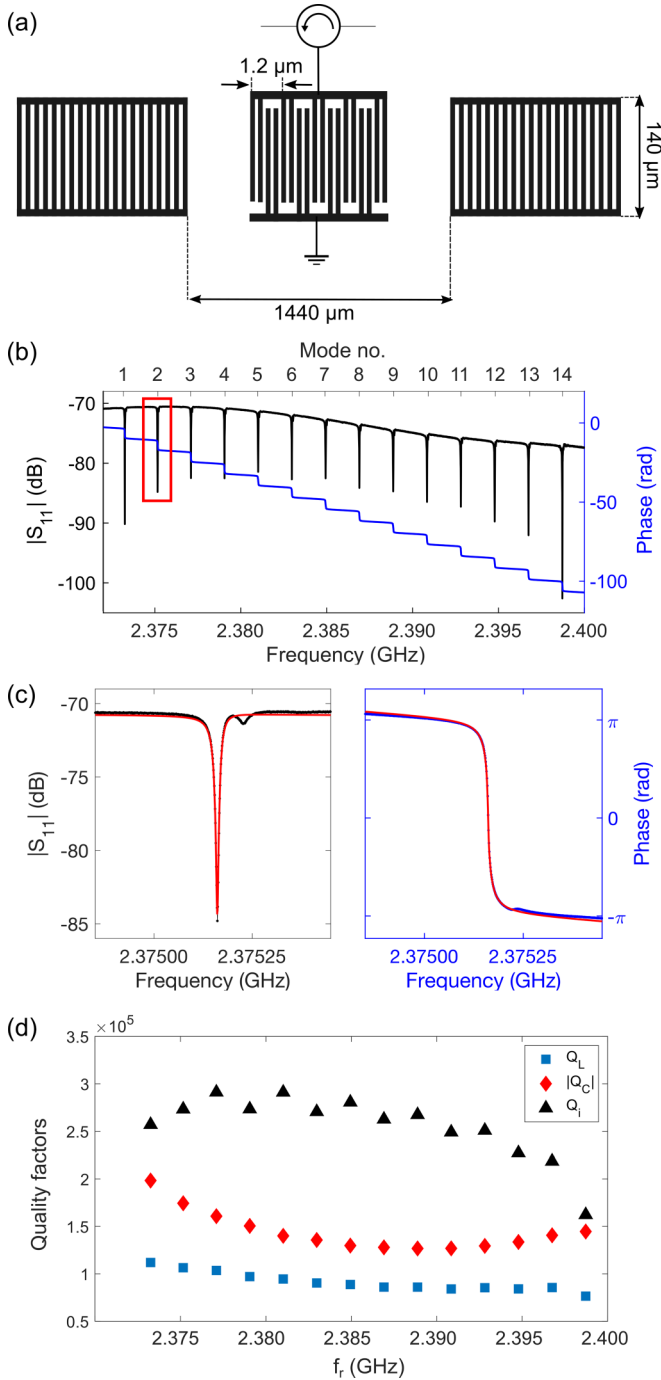
FIG. 1. (a) Dimensions of the SAW resonator used in this study (not to scale). The mirrors and the IDT are fabricated from aluminum patterned on a GaAs substrate. The shorted Bragg mirrors have 800 fingers each. The IDT has a split-finger design with 50 periods of 1.2 μm. (b) The reflection measurement of the SAW resonator, showing the 14 resonance modes lying between the frequency of 2.37 and 2.40 GHz. The indices represent mode numbers arranged from the lowest to the highest frequency of the resonator stop band. (c) The fitted magnitude and phase of resonance mode 2 highlighted by the red box in the top figure. The quality factors are extracted using Eq. (2). (d) SAW mode quality factors. The coupling coefficient Q_C ranges from 1.2×10^5 to 2.0×10^5, and the internal quality factor Q_i varies from 2.0×10^5 to 2.5×10^5.

We also observe time windows with large fluctuation features. These noise bursts appear randomly in our measurements separated in time by minutes or hours, as shown in Figs. 2(c)–2(e). In these periods, we recognize similar features in all traces, indicating significant correlations between them. Figure 2(c) shows a series of substantial frequency shifts followed by a relaxation tail. The shifts are negative in the low mode numbers. Their magnitude reduces as the mode number increases. Above mode 10, the frequency shift changes sign to positive, while the magnitude grows as the mode number increases further.

Figure 2(d) presents frequency noise with a large amplitude. At 4:48:35 h, we observe a frequency increase followed by a relaxation tail. This feature superimposes with a different frequency shift, which has a weaker amplitude and can be either positive or negative. While the burst event shows positive shifts in all modes, this second event has a negative sign in the first nine modes. Above mode 10, both shifts are positive, resulting in anomalously high amplitudes, on the order of a few kilohertz. In Fig. 2(e), we can see the characteristic of the noise of the second kind, where the magnitude gradually changes and switches signs. The magnitude of fluctuations decreases with increasing mode number before the frequency shift becomes positive, similar to the features observed in Fig. 2(c).

To determine the relationship between the frequency noise in different modes i and j, we compute the correlation coefficients C_{ij}, which is given by

$$C_{ij} = \frac{\langle \Delta f_i \Delta f_j \rangle}{\sqrt{\langle \Delta f_i^2 \rangle \langle \Delta f_j^2 \rangle}}, \qquad (3)$$

where $\langle \ \rangle$ denotes the expectation value. Figure 3(a) illustrates the correlation matrix of the frequency noise calculated from the entire measurement (7 h and 15 min). The frequency noise correlation reduces with increasing detuning, i.e., modes closer in frequency show stronger correlations than far-detuned modes. As suggested by Eq. (1), at a given frequency f_r, a TLS far from resonance contributes to the frequency noise less than a near-resonant TLS. Furthermore, we obtain negative correlations at a certain detuning, implying that two modes have frequency shifts in opposite directions. This result is not surprising, given that many large frequency shifts shown in Figs. 2(c)–2(e) explicitly show opposite signs.

Based on the STM, the anticorrelated noise bursts are not likely to be induced by TLSs. Under a continuous drive, near-resonant TLSs in the ground state can be excited by the SAW field. If TLSs are saturated, they do not contribute to resonance frequency shifts [29]. Thus, saturating TLSs in a specific part of the frequency spectrum will result in an effect similar to the removal of TLSs and their associated dispersive shift, pushing neighboring SAW modes toward the saturated region. The modes that are positively detuned from the saturated TLSs will experience negative frequency shifts, while those that are negatively detuned from the saturated TLSs will have positive shifts. Therefore, we would expect anticorrelated frequency shifts for the modes on opposite sides. Such frequency shifts caused by saturating TLSs are in the reverse direction to the results observed in our measurements.
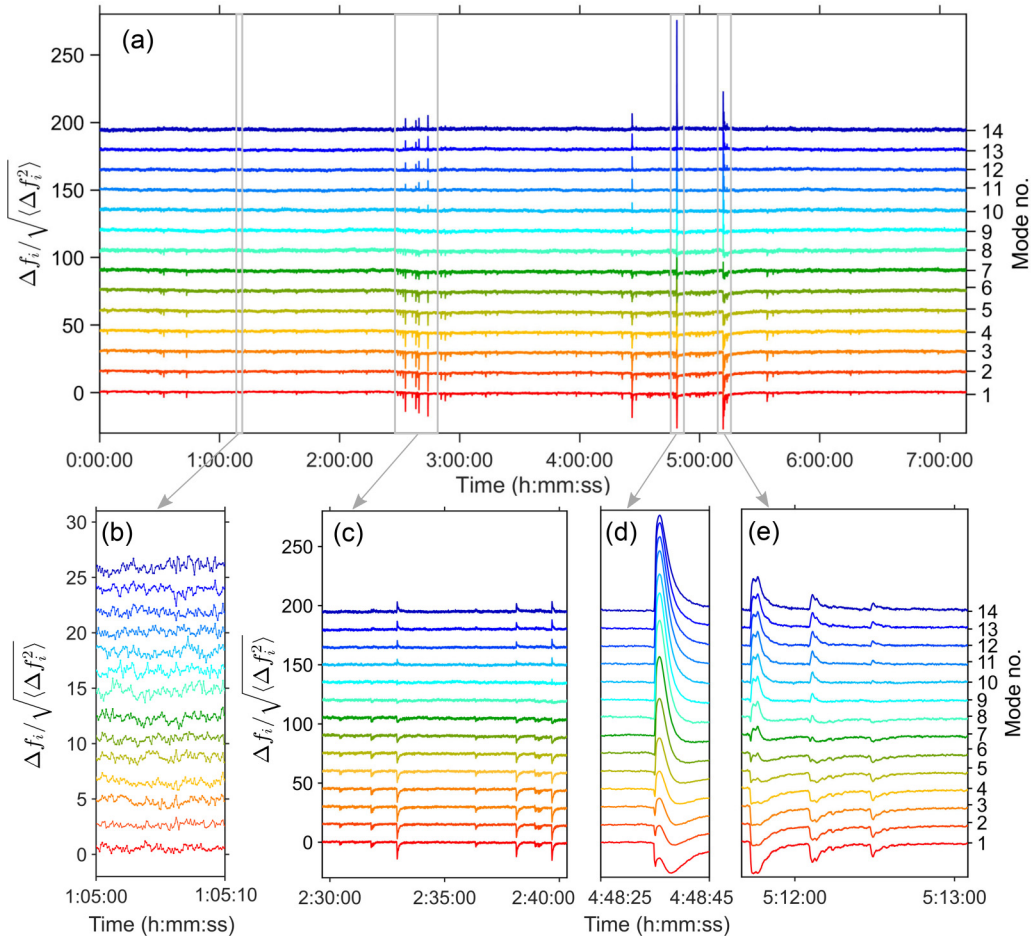
FIG. 2. (a) Normalized time traces of SAW resonance frequency fluctuations of the resonator mode 1 up to mode 14. All traces are measured simultaneously for approximately 7 h and 15 min. The traces are vertically shifted for better visualization. Bottom panel: Time traces in specific time windows highlighted by gray boxes in the top panel. (b) The resonance frequencies in the "quiet" time window where fluctuations are small. Note that the traces are shifted by a different proportion from (a). (c)–(e) The frequency noise in these time windows shows additional burst events superimposed with the TLS-induced noise. (See discussion in the main text.)

According to Eq. (1), the dispersive interaction between a resonator and a ground-state TLS will shift frequencies away from each other. These frequency shifts will give rise to negative correlation coefficients, which are similar to the effects observed in our experiment. Anticorrelated frequency noise could arise from the sudden appearance or elimination of TLSs at specific frequencies, and such "scrambling" of the TLS distribution has been observed with superconducting qubits [46]. That process, however, does not show the slow relaxation of mode frequencies observed here and is not consistent with stronger anticorrelations between further-detuned modes.

Considering the frequency noise only in a quiet period, we do not observe clear negative correlations, as shown in Fig. 3(b). From the correlation matrices, we can calculate the average correlation as a function of detuning between modes. Figure 3(c) shows that the correlation coefficients between all pairs of modes show a smooth variation. In the quiet time window, the noise correlation reduces from unity to zero. For the full time trace, the correlation switches its sign when the detuning exceeds 18 MHz. The diminishing positive correlation characteristic agrees with our current understanding of

the TLS interaction. However, this mechanism cannot explain the anticorrelations during the burst periods.

We further perform a frequency domain analysis by calculating the noise power spectral density S_f. We consider the standard power-law noise, where the noise spectrum is expressed by [47]

$$S_f(f) = \frac{h_{-1}}{f} + h_0. \qquad (4)$$

Here, h_{-1} and h_0 denote the $1/f$ and the white noise level, respectively. The power spectral density (PSD) of the frequency noise in mode 8 is plotted in Fig. 4. The PSD calculated from the quiet time window exhibits a $1/f$ characteristic, which is anticipated for the TLS-induced frequency noise [48]. For the full trace, where the frequency bursts are present, the PSD at low frequencies is one order of magnitude higher than that of the quiet window, indicating that the anomalous frequency fluctuations dominate in this frequency range. See Supplemental Material for the time-domain analysis [45]. We fit a sum of $1/f$ and Lorentzian frequency noise
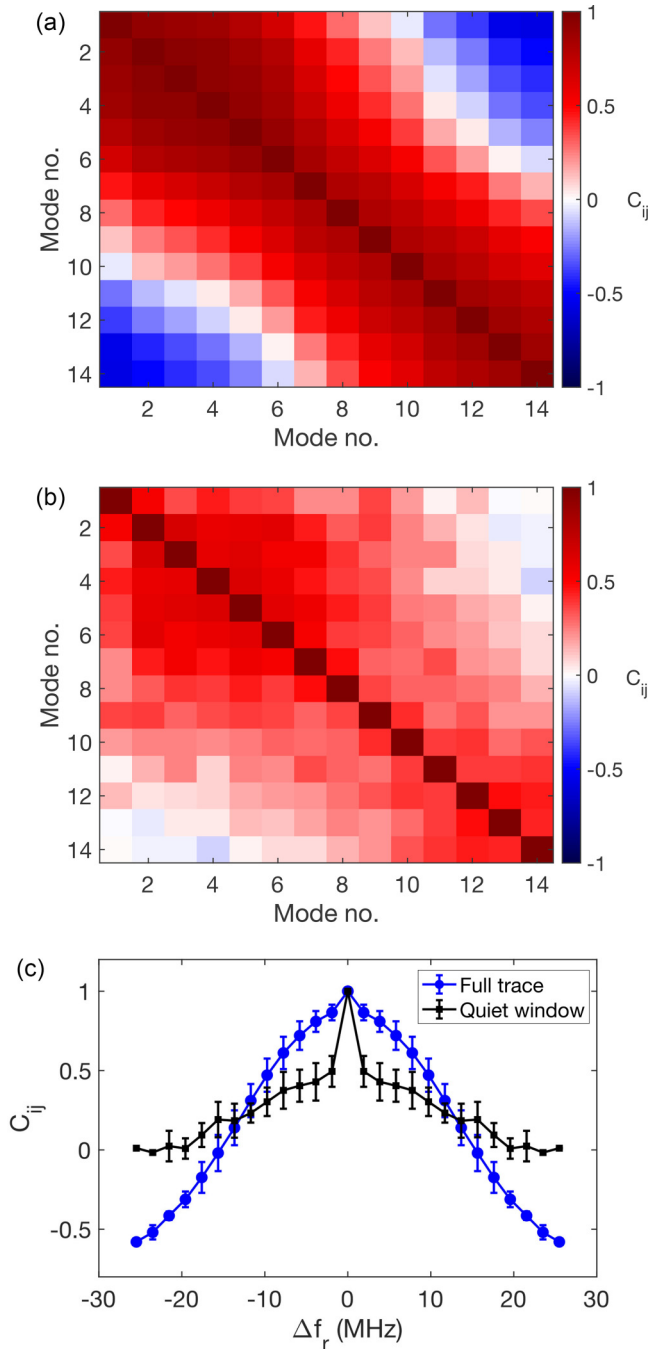
FIG. 3. (a) The matrix showing the correlation coefficients of the frequency noise measured for 7 h and 15 min, shown in Fig. 2(a). Note that the correlation diminishes and becomes negative when the pair of modes is far detuned. (b) The correlation matrix calculated from the quiet time window shown in Fig. 2(b). For this specific period, the correlations between modes still manifest a diminishing trend. However, we no longer observe clear negative correlations between modes. (c) Averaged correlation coefficients as a function of detuning calculated from the whole time trace (blue) and the quiet window (black). For the correlations of the full time trace, the sign of the correlation switches from positive to negative when the detuning is approximately 18 MHz. Note that the plot is symmetric as $C_{ij} = C_{ji}$.
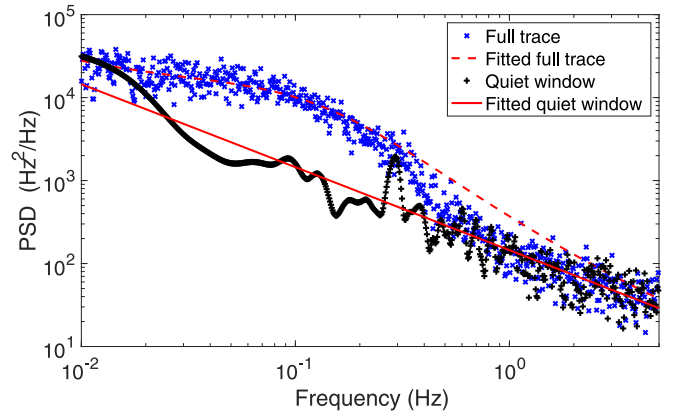

FIG. 4. Noise power spectral density of the frequency fluctuations in mode 8 calculated from the entire trace and from the quiet time window only (approximately 400 s long). The lines represent the fitted power-law noise model [Eq. (4)] and the sum of the power-law noise and the Lorentzian noise model [Eq. (4) + Eq. (5)].

$$\text{PSD}(f) = S_L(f) + S_f(f), \text{ where}$$

$$S_L(f) = \frac{4A^2\tau_0}{1 + (2\pi f \tau_0)^2}. \tag{5}$$

Here, A and τ_0 are the Lorentzian noise amplitude and the characteristic timescale, respectively. With this model, we obtain the Lorentzian noise amplitude $A = 53.12$ Hz, the Lorentzian characteristic time $\tau_0 = 1.22$ s, the $1/f$ noise power $h_{-1} = 145.0$ Hz^2, whereas the white noise level is negligible. The characteristic time falls in the range of the characteristic time of relaxation tails 1.2–3.0 s, observed in the time traces in Fig. 2. This fit does not capture the steep rolloff of the PSD at higher frequencies, indicating a non-Lorentzian spectrum of the slow frequency excursions. Our analysis in both time and frequency domains suggests that the frequency noise cannot be purely induced by TLSs and the large fluctuations are caused by an additional noise source.

As shown in Fig. 2, frequency noise anomalies have an abrupt change followed by a relaxation tail. This characteristic resembles the effect of ionizing radiation in high-kinetic inductance superconducting devices caused by cosmic rays [37]. In that case, the long-time transient effects are due to long recombination times of quasiparticles above the superconducting gap, a mechanism absent in our mechanical resonator. The expected flux of high-energy cosmic muons is around 10 per hour across the chip cross section [7,37,49], a rate consistent with our data, although there is no obvious interaction mechanism. An ionization event induced by radiation could lead to the generation of electron-hole pairs which get trapped in deep-level defects with long relaxation times similar to the timescale of observed fluctuations [50,51]. The correlations of the frequency noise between different modes vary smoothly with detuning and show a uniform behavior where the signs of frequency excursions are consistent across

different events. This suggests a geometrical effect arising from the spatial distribution of a single or small number of defects and the acoustic field variation with mode number. Further investigation is necessary in order to pin down the origin of anticorrelated fluctuations.

In conclusion, we have reported two distinctive noise processes in a surface acoustic wave resonator. There is TLS-induced noise, showing diminishing correlations with increased detuning and a noise spectral density with $1/f$ characteristics. This noise signature provides additional evidence for TLSs as the origin of phase noise in quantum devices. The correlated nature of phase noise suggests that quantum information encoded in different modes of the same resonator undergo reduced relative dephasing. In the presence of TLS noise, a multimode quantum memory may therefore provide improved preservation of entanglement compared to physically separated modes. Additionally, we observe anomalous frequency fluctuations, whose origins are not clear but show some resemblance to the previously observed impact of cosmic radiation. Our multimode probe scheme reveals

striking negative correlations in these fluctuations, whose noise power spectral densities are approximately represented by a Lorentzian noise model.

N.T. performed the measurements and analysis, N.T. and G.A. developed the conceptual idea behind the experiment, J.H.C. provided theory support, P.D. and G.A. supervised the project, and N.T. wrote the manuscript with input from all coauthors.

The authors declare no competing interests.

---

[1] R. W. Simmonds, K. M. Lang, D. A. Hite, S. Nam, D. P. Pappas, and J. M. Martinis, Phys. Rev. Lett. **93**, 077003 (2004).

[2] J. J. Burnett, A. Bengtsson, M. Scigliuzzo, D. Niepce, M. Kudra, P. Delsing, and J. Bylander, NPJ Quantum Inf. **5**, 54 (2019).

[3] C. Müller, J. Lisenfeld, A. Shnirman, and S. Poletto, Phys. Rev. B **92**, 035442 (2015).

[4] J. M. Martinis, K. B. Cooper, R. McDermott, M. Steffen, M. Ansmann, K. D. Osborn, K. Cicak, S. Oh, D. P. Pappas, R. W. Simmonds, and C. C. Yu, Phys. Rev. Lett. **95**, 210503 (2005).

[5] C. D. Wilen, S. Abdullah, N. A. Kurinsky, C. Stanford, L. Cardani, G. D'Imperio, C. Tomei, L. Faoro, L. B. Ioffe, C. H. Liu, A. Opremcak, B. G. Christensen, J. L. DuBois, and R. McDermott, Nature (London) **594**, 369 (2021).

[6] R. Barends, J. Wenner, M. Lenander, Y. Chen, R. C. Bialczak, J. Kelly, E. Lucero, P. O'Malley, M. Mariantoni, D. Sank, H. Wang, T. C. White, Y. Yin, J. Zhao, A. N. Cleland, J. M. Martinis, and J. J. A. Baselmans, Appl. Phys. Lett. **99**, 113507 (2011).

[7] A. P. Vepsäläinen, A. H. Karamlou, J. L. Orrell, A. S. Dogra, B. Loer, F. Vasconcelos, D. K. Kim, A. J. Melville, B. M. Niedzielski, J. L. Yoder, S. Gustavsson, J. A. Formaggio, B. A. VanDevender, and W. D. Oliver, Nature (London) **584**, 551 (2020).

[8] J. Burnett, L. Faoro, V. G. I. Wisby, A. Chernykh, G. Mikhailov, V. Tulin, R. Shaikhaidarov, V. Antonov, P. Meeson, A. Tzalenchuk, and T. Linström, Nat. Commun. **5**, 4119 (2014).

[9] C. Müller, J. Cole, and J. Lisenfeld, Rep. Prog. Phys. **82**, 124501 (2019).

[10] P. V. Klimov, J. Kelly, Z. Chen, M. Neeley, A. Megrant, B. Burkett, R. Barends, K. Arya, B. Chiaro, Y. Chen, A. Dunsworth, A. Fowler, B. Foxen, C. Gidney, M. Giustina, R. Graff, T. Huang, E. Jeffrey, E. Lucero, J. Y. Mutus *et al.*, Phys. Rev. Lett. **121**, 090502 (2018).

[11] S. Matityahu, A. Shnirman, and M. Schechter, Phys. Rev. Appl. **16**, 044036 (2021).

[12] X. You, Z. Huang, U. Alyanak, A. Romanenko, A. Grassellino, and S. Zhu, Phys. Rev. Appl. **18**, 044026 (2022).

[13] B. Chiaro, A. Megrant, A. Dunsworth, Z. Chen, R. Barends, B. Campbell, Y. Chen, A. Fowler, I. C. Hoi, E. Jeffrey, J. Kelly, J. Mutus, C. Neill, P. J. J. O'Malley, C. Quintana, P. Roushan, D. Sank, A. Vainsencher, J. Wenner, T. C. White, and J. M. Martinis, Supercond. Sci. Technol. **29**, 104006 (2016).

[14] J. Koch, T. M. Yu, J. Gambetta, A. A. Houck, D. I. Schuster, J. Majer, A. Blais, M. H. Devoret, S. M. Girvin, and R. J. Schoelkopf, Phys. Rev. A **76**, 042319 (2007).

[15] K. Cicak, D. Li, J. A. Strong, M. S. Allman, F. Altomare, A. J. Sirois, J. D. Whittaker, J. D. Teufel, and R. W. Simmonds, Appl. Phys. Lett. **96**, 093502 (2010).

[16] J. B. Chang, M. R. Vissers, A. D. Córcoles, M. Sandberg, J. Gao, D. W. Abraham, J. M. Chow, J. M. Gambetta, M. Beth Rothwell, G. A. Keefe, M. Steffen, and D. P. Pappas, Appl. Phys. Lett. **103**, 012602 (2013).

[17] J. Lisenfeld, A. Bilmes, A. Megrant, R. Barends, J. Kelly, P. Klimov, G. Weiss, J. M. Martinis, and A. V. Ustinov, NPJ Quantum Inf. **5**, 105 (2019).

[18] W. Phillips, J. Low Temp. Phys. **7**, 351 (1972).

[19] P. W. Anderson, B. I. Halperin, and C. M. Varma, Philos. Mag. **25**, 1 (1972).

[20] L. Faoro and L. B. Ioffe, Phys. Rev. B **91**, 014201 (2015).

[21] J. Lisenfeld, G. J. Grabovskij, C. Müller, J. H. Cole, G. Weiss, and A. V. Ustinov, Nat. Commun. **6**, 6182 (2015).

[22] J. L. Black and B. I. Halperin, Phys. Rev. B **16**, 2879 (1977).

[23] J. Gao, J. Zmuidzinas, B. A. Mazin, H. G. LeDuc, and P. K. Day, Appl. Phys. Lett. **90**, 102507 (2007).

[24] D. Niepce, J. J. Burnett, M. Kudra, J. H. Cole, and J. Bylander, Sci. Adv. **7**, eabh0462 (2021).

[25] G. J. Grabovskij, T. Peichl, J. Lisenfeld, G. Weiss, and A. V. Ustinov, Science **338**, 232 (2012).

[26] J. Gao, M. Daal, A. Vayonakis, S. Kumar, J. Zmuidzinas, B. Sadoulet, B. Mazin, P. Day, and H. Leduc, Appl. Phys. Lett. **92**, 152505 (2008).

[27] D. P. Pappas, M. R. Vissers, D. S. Wisbey, J. S. Kline, and J. Gao, IEEE Trans. Appl. Supercond. **21**, 871 (2011).

[28] D. V. Anghel, T. Kühn, Y. M. Galperin, and M. Manninen, Phys. Rev. B **75**, 064202 (2007).

[29] G. Andersson, A. L. Bilobran, M. Scigliuzzo, M. M. de Lima, J. H. Cole, and P. Delsing, NPJ Quantum Inf. **7**, 15 (2021).

[30] A. Y. Cleland, E. A. Wollack, and A. H. Safavi-Naeini, arXiv:2302.00221.

[31] R. Manenti, M. J. Peterer, A. Nersisyan, E. B. Magnusson, A. Patterson, and P. J. Leek, Phys. Rev. B **93**, 041411(R) (2016).

[32] E. Jaynes and F. Cummings, Proc. IEEE **51**, 89 (1963).

[33] L. Grünhaupt, N. Maleeva, S. T. Skacel, M. Calvo, F. Levy-Bertrand, A. V. Ustinov, H. Rotzinger, A. Monfardini, G. Catelani, and I. M. Pop, Phys. Rev. Lett. **121**, 117001 (2018).

[34] L. J. Swenson, A. Cruciani, A. Benoit, M. Roesch, C. S. Yung, A. Bideaud, and A. Monfardini, Appl. Phys. Lett. **96**, 263511 (2010).

[35] D. C. Moore, S. R. Golwala, B. Bumble, B. Cornell, P. K. Day, H. G. LeDuc, and J. Zmuidzinas, Appl. Phys. Lett. **100**, 232601 (2012).

[36] G. Catelani, R. J. Schoelkopf, M. H. Devoret, and L. I. Glazman, Phys. Rev. B **84**, 064517 (2011).

[37] L. Cardani, F. Valenti, N. Casali, G. Catelani, T. Charpentier, M. Clemenza, I. Colantoni, A. Cruciani, G. D'Imperio, L. Gironi, L. Grünhaupt, D. Gusenkova, F. Henriques, M. Lagoin, M. Martinez, G. Pettinari, C. Rusconi, O. Sander, C. Tomei, A. V. Ustinov *et al.*, Nat. Commun. **12**, 2733 (2021).

[38] S. E. de Graaf, L. Faoro, L. B. Ioffe, S. Mahashabde, J. J. Burnett, T. Lindström, S. E. Kubatkin, A. V. Danilov, and A. Y. Tzalenchuk, Sci. Adv. **6**, eabc5055 (2020).

[39] M. McEwen, L. Faoro, K. Arya, A. Dunsworth, T. Huang, S. Kim, B. Burkett, A. Fowler, F. Arute, J. C. Bardin, A. Bengtsson, A. Bilmes, B. B. Buckley, N. Bushnell, Z. Chen, R. Collins, S. Demura, A. R. Derk, C. Erickson, M. Giustina *et al.*, Nat. Phys. **18**, 107 (2022).

[40] P. Astone, M. Bassan, P. Bonifazi, P. Carelli, E. Coccia, S. D'Antonio, V. Fafone, G. Federici, A. Marini, G. Mazzitelli, Y. Minenkov, I. Modena, G. Modestino, A. Moleti, G. Pallottino, V. Pampaloni, G. Pizzella, L. Quintieri, F. Ronga, R. Terenzi *et al.*, Phys. Lett. B **499**, 16 (2001).

[41] P. Astone, D. Babusci, M. Bassan, P. Bonifazi, G. Cavallari, E. Coccia, S. D'Antonio, V. Fafone, G. Giordano, C. Ligi, A. Marini, G. Mazzitelli, Y. Minenkov, I. Modena, G. Modestino, A. Moleti, G. Pallottino, G. Pizzella, L. Quintieri, A. Rocchi *et al.*, Astropart. Phys. **30**, 200 (2008).

[42] M. Goryachev, W. M. Campbell, I. S. Heng, S. Galliou, E. N. Ivanov, and M. E. Tobar, Phys. Rev. Lett. **127**, 071102 (2021).

[43] K. Karatsu, A. Endo, J. Bueno, P. J. de Visser, R. Barends, D. J. Thoen, V. Murugesan, N. Tomita, and J. J. A. Baselmans, Appl. Phys. Lett. **114**, 032601 (2019).

[44] S. Probst, S. Song, P. Bushev, A. Ustinov, and M. Weides, Rev. Sci. Instrum. **86**, 024706 (2015).

[45] See Supplemental Material at http://link.aps.org/supplemental/10.1103/PhysRevB.109.L241301 for the experimental setup; phase fluctuation time traces of the control tone and all SAW modes; time-domain analysis showing Allan deviation plots of the resonance frequency fluctuations calculated from the data in Fig. 2; and power dependence of the frequency noise, which includes Refs. [23,47,52–55].

[46] T. Thorbeck, A. Eddins, I. Lauer, D. T. McClure, and M. Carroll, PRX Quantum **4**, 020356 (2023).

[47] E. Rubiola, Phase noise and feedback theory, in *Phase Noise and Frequency Stability in Oscillators*, The Cambridge RF and Microwave Engineering Series (Cambridge University Press, Cambridge, U.K., 2008), pp. 88–124.

[48] J. Burnett, T. Lindström, M. Oxborrow, Y. Harada, Y. Sekine, P. Meeson, and A. Y. Tzalenchuk, Phys. Rev. B **87**, 140501(R) (2013).

[49] S. Tsuji, T. Katayama, K. Okei, T. Wada, I. Yamamoto, and Y. Yamashita, J. Phys. G: Nucl. Part. Phys. **24**, 1805 (1998).

[50] R. Zuleeg, Radiation effects in GaAs integrated circuits, in *GaAs Microelectronics*, edited by N. G. Einspruch and W. R. Wisseman, VLSI Electronics Microstructure Science (Academic Press, Orlando, FL, 1985), Vol. 11, Chap. 11, pp. 391–436.

[51] A. R. Peaker, V. P. Markevich, and J. Coutinho, J. Appl. Phys. **123**, 161559 (2018).

[52] C. M. Van Vliet and P. H. Handel, Phys. A: Stat. Mech. Appl. **113**, 261 (1982).

[53] J. A. Barnes, A. R. Chi, L. S. Cutler, D. J. Healey, D. B. Leeson, T. E. McGunigal, J. A. Mullen, W. L. Smith, R. L. Sydnor, R. F. C. Vessot, and G. M. R. Winkler, IEEE Trans. Instrum. Meas. **IM-20**, 105 (1971).

[54] R. Barends, N. Vercruyssen, A. Endo, P. J. de Visser, T. Zijlstra, T. M. Klapwijk, and J. J. A. Baselmans, Appl. Phys. Lett. **97**, 033507 (2010).

[55] J. Gao, M. Daal, J. M. Martinis, A. Vayonakis, J. Zmuidzinas, B. Sadoulet, B. A. Mazin, P. K. Day, and H. G. Leduc, Appl. Phys. Lett. **92**, 212504 (2008).